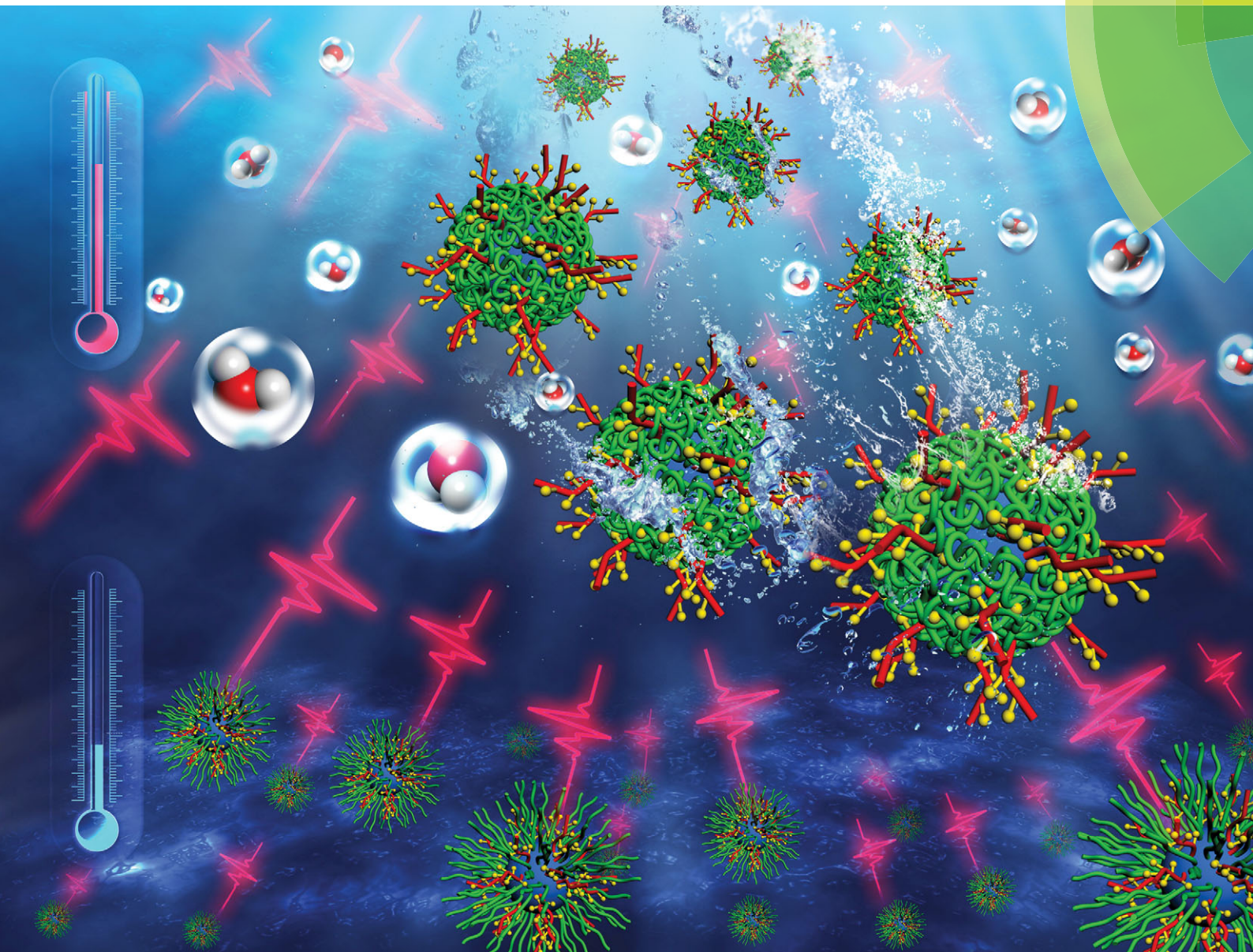


ChemComm

Chemical Communications

www.rsc.org/chemcomm



ISSN 1359-7345



ROYAL SOCIETY
OF CHEMISTRY

COMMUNICATION

Xin Zhou *et al.*

Body temperature sensitive micelles for MRI enhancement

COMMUNICATION



Body temperature sensitive micelles for MRI enhancement†

Xiaolei Zhu, Shizhen Chen, Qing Luo, Chaohui Ye, Maili Liu and Xin Zhou*

 Cite this: *Chem. Commun.*, 2015, 51, 9085

 Received 29th March 2015,
Accepted 2nd April 2015

DOI: 10.1039/c5cc02587g

www.rsc.org/chemcomm

A novel thermo-sensitive micelle contrast agent and its enhancement of MRI contrast with temperature are reported. The morphology changes sharply near 37 °C, resulting in a significant amplification of the CEST signal. This enables detection of small changes in body temperature.

The temperature difference between tissues is a common feature in pathological conditions, especially in tumors. Because of the Warburg effect, the production of energy within the tumor generally exceeds that within normal tissue.^{1,2} Malignant cells and rapidly growing blood vessels are found in tumor micro-environments. Such features make the tumor tissue's temperature, pH, and other metabolites significantly different from those of normal tissue.^{3,4} Therefore, the tissue temperature measurements *in vivo* are valuable biomarkers for disease detection. Also, methods to monitor local heating effects are relevant in thermally activated drug delivery, or during treatments such as hyperthermic ablation of tumors.^{5,6} At present, however, no good methods exist for non-invasively mapping tissue temperatures *in vivo* over small ranges. Magnetic resonance imaging (MRI), which is a well-known non-invasive diagnostic tool for anatomical imaging, can report on physiological changes in tissue. This characteristic makes MRI a powerful tool for tumor detection and orientation.^{7,8}

Due to the intrinsically low sensitivity of MRI signal detection in comparison to other analytical techniques, various methods for signal enhancement and optimization have been investigated.^{9–11} An interesting alternative method to generate the contrast enhancement for MRI is chemical exchange saturation transfer (CEST), which can amplify the signal of protein-bound water by the bulk water through proton exchange between these two pools.^{11,12} Furthermore, paramagnetic CEST (PARACEST) contrast agents are used to measure physiological parameters, including tissue pH

based on its dependence on the exchange rate between bound protons and bulk protons, and tissue temperature based on its dependence on the exchangeable proton's chemical shift.^{13–16} However, the MRI sensitivity is still limited because of the tiny difference between normal and abnormal tissues.

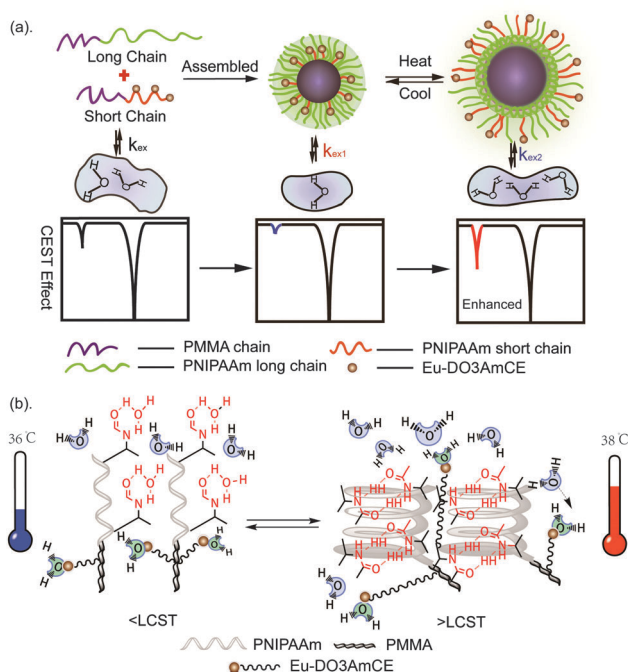
In order to enhance the imaging contrast for temperature changes, we developed a novel PARACEST MRI contrast agent based on a responsive polymeric micelle system.^{17–19} A smart copolymer PNIPAAm-*b*-MMA (poly *N*-isopropylacrylamide block methyl methacrylate) chain was chosen self-assembling as a core-shell thermal-responsive micelle.^{20,21} The morphology of the thermo-responsive micelle is sensitive to the temperature changes at its lower critical solution temperature (LCST). Such a micelle can be delivered to the target tumor, and trigger the release of a drug or a contrast agent *via* thermal activation. It was hypothesized that the temperature-dependent morphology change of the micelle, especially around the LCST, would heavily influence the CEST effect of MRI.^{22,23} Therefore, CEST MRI could be used to visualize temperature variations in the human body.

In order to demonstrate this hypothesis, a smart mixed micelle, a composite of two kinds of unimer chains, long chain and short chain, was used. The short chain was modified by linking a PARACEST agent of europium(III) tetra amide complex (EuDOTA-4AmCE) *via* diamine. As shown in Scheme 1(a), the different lengths of amphiphilic chains self-assemble as a core-shell micelle. The hydrophobic PMMA (poly-methyl methacrylate) chains form a core, while the hydrophilic PNIPAAm chains form a shell under the synergistic effect. In addition, the PNIPAAm chains exhibit a reversible thermo-responsive phase transition in aqueous solution.

Accordingly, when the temperature is lower than the micelle's LCST, the stretched hydrophilic chains embed the contrast agents in the micelle. When the temperature is above the LCST, the micelle's hydrophilic chains fold as an aggregated cluster, causing the exposure of short chains modified with Eu-DOTAmCE to the bulk water, as illustrated in Scheme 1(b). It therefore makes sense to design and synthesize such a novel polymeric micelle with a LCST located at the human body temperature to create a

Key Laboratory of Magnetic Resonance in Biological Systems, State Key Laboratory of Magnetic Resonance and Atomic and Molecular Physics, National Center of Magnetic Resonance in Wuhan, Wuhan Institute of Physics and Mathematics, Chinese Academy of Sciences, Wuhan 430071, China. E-mail: xinzhou@wipm.ac.cn

† Electronic supplementary information (ESI) available: (1) General experimental section; (2) characterization and CEST experimental section. See DOI: 10.1039/c5cc02587g



Scheme 1 (a) A schematic diagram of the CEST MRI signal changes in response to the micelle's morphological changes. (b) The temperature change around the LCST affecting the PNIPAAm chain, which is folded as an aggregated cluster when the temperature is higher than the LCST of 37 °C.

temperature reporter in the vicinity of this temperature. Due to the morphological alternation of the micelle induced by the temperature, it will affect the interaction between the bulk water and the PARCEST agent, and then cause an MRI signal modulation by the temperature.

The polymeric micelle modified with the PARCEST agent was synthesized by a simple procedure (Fig. S1, ESI[†]), resulting in the Eu-[PNIPAAm-MMA-DO3AmCE] complex. After this, Eu-[PNIPAAm-MMA-DO3AmCE] was mixed with the unmodified polymers with long chains to prepare a core-shell micelle. Ten different micelle concentrations contained in a pyrene probe have been used to derive the critical micelle concentration (CMC). The experiments showed that the intensity of the pyrene fluorescence (I_3/I_1) increased dramatically when the concentration was above 10 $\mu\text{g ml}^{-1}$, which is considered to be its CMC (Fig. S2, ESI[†]).

We have used dynamic light scattering (DLS) and transmission electron microscopy (TEM) to characterize the size and morphology of the Eu-[PNIPAAm-MMA-DO3AmCE] micelle both in solution and in the solid-state, by evaporating the solvent. As shown in Fig. 1a, the diameter distribution of micelles determined using a laser particle size analyzer was quite narrow, and the mean size of micelles at 37 °C was 99.6 nm. TEM images (Fig. 1b and its inset) show the spherical nature of the Eu-[PNIPAAm-MMA-DO3AmCE] micelles, which is consistent with the results observed by dynamic light scattering. This indicates that the core-shell structure of micelles and the shell of the hydrophilic PNIPAAm chains prevent the formation of intermicellar aggregates. Moreover, the quantitative analysis of europium ions (Eu^{3+}) of the micelle was characterized as 10 mM per 11 mg ml^{-1} micelle by inductively coupled plasma-mass

spectrometry (ICP-MS, X Series 2, Thermo Fisher Scientific, Inc.). The temperature dependence of the hydrodynamic diameter of the micelle is shown in Fig. 1(c). A remarkable change was observed at around 36 °C to 38 °C and no appreciable change occurred at around 32 °C to 36 °C. This illustrated that the phase transition of thermo-responsive chains has been triggered at around 37 °C, which is in agreement with the LCST. Optical transmittance tests were carried out at 542 nm using a SpectraMax 190 Microplate Reader (Molecular Devices, USA), equipped with a temperature-controllable cell. The temperature ranged from 33 °C to 42 °C with intervals of 1 °C. The sample was equilibrated for 15 min before each measurement, as shown in Fig. 1(d). The optical transmittance of the micelle solution showed a significant decrease from 36 °C to 38 °C, at an excitation wavelength of 542 nm. In response to temperatures above the LCST of 37 °C, the micelles form hydrophobic globules due to polymer dehydration. Furthermore, these physicochemical and structural changes in PNIPAAm polymers reversibly occur across the LCST in the aqueous phase.

NMR measurements were implemented on a Bruker Avance 500 MHz (11.7 T) spectrometer with a variable temperature controller. The basic pulse sequence of the CEST experiment consisted of a continuous presaturation pulse (B_1) followed by a hard 90-degree pulse. To optimize the experimental parameters, the presaturation time (T_S) ranged from 0 to 15 s, and the presaturation power ranged from 0 to 25 μT . The CEST spectra were acquired to measure the CEST effect by recording the bulk water signal intensity as a function of presaturation frequency from -70 ppm to +70 ppm using a step size of 1 ppm. To verify the CEST enhancement of the micelle contrast relative to the conventional PARCEST agent (Eu-DOTA-4AmC⁻), the Z-spectra for both samples were recorded under the identical conditions (Fig. S3, ESI[†]). Eu-[PNIPAAm-MMA-DO3AmCE] displayed a marked saturation contrast effect at a presaturation frequency of 54.9 ppm. This corresponds to the saturation of the bound water peak at 54.9 ppm, which is transferred into the bulk water and decreases the signal acquired at 0 ppm. However, the unmodified polymers did not show any appreciable saturation contrast at this frequency. The CEST contrast is generated by the saturation of the exchangeable chemically shifted bound water pool associated with a PARCEST agent using a long continuous wave radio frequency pulse. These saturated protons then transfer to the bulk water pool by chemical exchange. The net transfer of high-energy protons to the bulk proton pool leads to the reduction of the bulk water net magnetization, and therefore produces a negative contrast in MRI images.

The CEST effect was calculated according to the magnetization transfer ratio ($\text{MTR} = (\text{MS}^- - \text{MS}^+)/\text{MS}^-$), in which MS^+ is the magnitude of the bulk water signal during saturation in resonance, and MS^- is the intensity of the bulk water signal when saturated at the opposite frequency offset. To obtain the best MTR intensity of the micelle system, we have optimized the duration time and the presaturation power (shown in Fig. S4 and S5, ESI[†]). In order to demonstrate the temperature dependence of the CEST enhancement, the CEST spectra of a 10 mM Eu^{3+} polymeric micelle were acquired at different temperatures. As plotted in Fig. 2, the MTR of the Eu-[PNIPAAm-MMA-DO3AmCE]

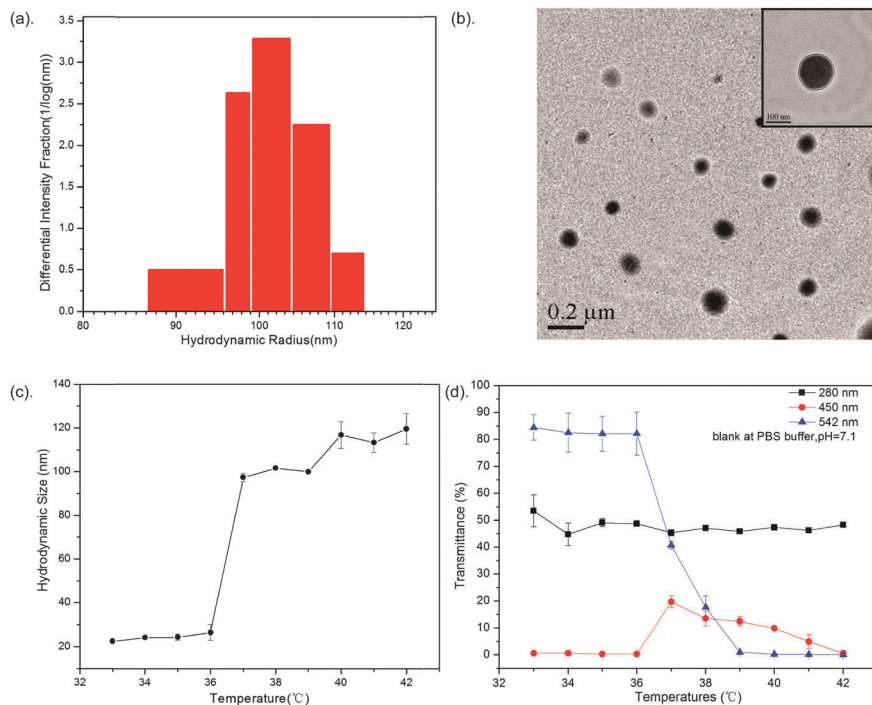


Fig. 1 (a) The hydrodynamic diameter distribution was measured by the dynamic lighting scattering at 37 °C. (b) The micelle's morphology characterized by transmission electron microscopy (TEM), and the inset showing a micelle with a core-shell structure of 100 nm. (c) The hydrodynamic diameter distribution of micelle as a function of temperature by the dynamic lighting scattering. (d) Light transmittance at different temperatures for different absorption wavelengths (542 nm, 450 nm, 280 nm), indicating the micelle's LCST of 37 °C at 542 nm.

micelle is strongly temperature dependent, as expected. When the temperature increased at around the LCST of 37 °C, a dramatic CEST enhancement was observed. Upon further increasing the temperature, the CEST signal decreased.

As far as we know, the lanthanide induced chemical shift effect and its CEST enhancement of the normal PARACEST agent are not sensitive to temperature over such a narrow range

of temperatures. However, this phenomenon due to the change in temperature at around the LCST significantly altered the morphology of the micelle (Fig. S6, ESI[†]), resulting in the change in retention time of the bound water. The retention time is the reciprocal of the exchange rate, which is the critical factor of the CEST enhancement. At room temperature, the retention time of the bound water in the micelle solution is about 120 μ s, as calculated by the multiple pool model,^{24,25} and it decreases with a higher temperature.¹⁵ As the hydrophilic chains of the PNIPAAm were stretched to form the outer shell, the isopropylamine could form hydrogen bonds with the free water, and the microenvironment tends to induce a slower chemical exchange rate with the bound water. When the temperature increased higher than the LCST, the outer shell gradually became hydrophobic and cross-linked to form clusters. The change in morphology provided more contact sites between the bound water and free water, resulting in the changes in the proton exchange rate and the CEST enhancement. As the temperature increased continuously, the morphology of the micelle became more stable and the CEST enhancement decreased slowly. To further verify this mechanism, phantom CEST images were obtained at different temperatures.

To demonstrate the thermally-sensitive CEST enhancement of the micelle, the CEST MR phantom images at different temperatures were obtained (Fig. 3). MR images were acquired at different temperatures and pH 6.8 on a Bruker Biospin 9.4 T micro-imaging scanner. A fast low-angle shot (FLASH) pulse sequence was used with TR/TE = 5012/6 ms, and the presaturation pulse was set at a frequency of 54 ppm with a power of 8 μ T

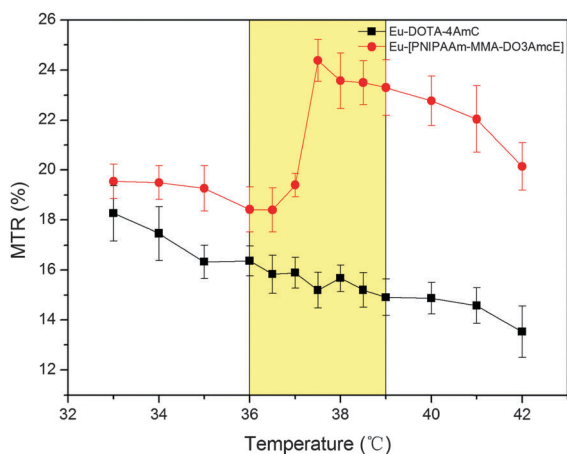


Fig. 2 Temperature dependence of the CEST enhancement (in MTR) for the micelle Eu-[PNIPAAm-MMA-DO3AmCE] (red) and the conventional PARACEST contrast agent Eu-DOTA-4AmC⁻ (black), respectively. Both of them have the same Eu³⁺ concentration of 10 mM, and the region of interest around the LCST is highlighted in yellow.

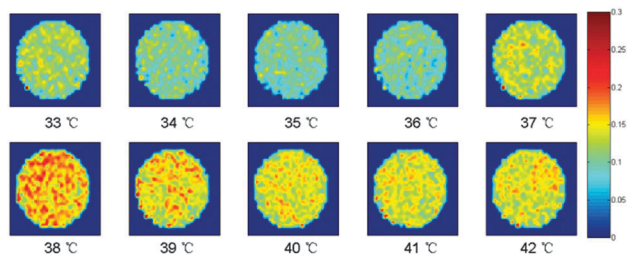


Fig. 3 The CEST MR phantom images (FOV = 20 × 20 mm²) at different temperatures obtained using a 9.4 T micro-imaging system with a saturation pulse of 8 μ T for 5 s. All the samples contained 21 mg l⁻¹ of micelles with an Eu³⁺ concentration of 10 mM, in pH 6.8 PBS solution. The CEST enhancement between 33 °C and 42 °C was scaled by the MTR value.

and a duration time of 8 s. The temperature change from 33 to 36 °C caused only a moderate variation in the CEST effect of the micelle. However, when the temperature exceeded 37 °C, the CEST MRI signal showed an obvious enhancement, and the maximum enhancement occurred at 38 °C, which are in agreement with the results of the CEST spectra. As the micelle's LCST was nearby the human body temperature, the CEST enhanced NMR and MRI methods may open a new way for hypersensitive detection of temperature change in different tissues.

In summary, a novel approach has been developed to detect body temperature by using the thermal-sensitive CEST enhancement of the PARACEST micelle Eu-[PNIPAAm-MMA-DO3AmCE]. Unlike the conventional PARACEST agent, Eu-DOTA-4AmCE, whose CEST effect decreased with increasing temperature in the physiological range, the CEST effect of Eu-[PNIPAAm-MMA-DO3AmCE] was significantly enhanced at body temperature. Due to its smart features, this thermo-sensitive micelle system may be useful for detection of temperature changes under abnormal conditions or during hyperthermia treatment.

This work was supported by the Natural Science Foundation of China (81227902, 21305156, 21221064 and 21120102038) and the Chinese Academy of Sciences (KJCX2-EW-N06-04).

Notes and references

- 1 M. R. Junttila and F. J. de Sauvage, *Nature*, 2013, **501**, 346–354.
- 2 R. J. Gillies, N. Raghunand, G. S. Karczmar and Z. M. Bhujwala, *J. Magn. Reson. Imaging*, 2002, **16**, 430–450.
- 3 S. Mura, J. Nicolas and P. Couvreur, *Nat. Mater.*, 2013, **12**, 991–1003.
- 4 D. Peer, J. M. Karp, S. Hong, O. C. Farokhzad, R. Margalit and R. Langer, *Nat. Nanotechnol.*, 2007, **2**, 751–760.
- 5 M. A. C. Stuart, W. T. S. Huck, J. Genzer, M. Muller, C. Ober, M. Stamm, G. B. Sukhorukov, I. Szleifer, V. V. Tsukruk, M. Urban, F. Winnik, S. Zauscher, I. Luzinov and S. Minko, *Nat. Mater.*, 2010, **9**, 101–113.
- 6 M. G. Vander Heiden, *Nat. Rev. Drug Discovery*, 2011, **10**, 671–684.
- 7 J.-H. Lee, Y.-M. Huh, Y.-W. Jun, J.-W. Seo, J.-T. Jang, H.-T. Song, S. Kim, E.-J. Cho, H.-G. Yoon, J.-S. Suh and J. Cheon, *Nat. Med.*, 2007, **13**, 95–99.
- 8 J. A. Barreto, W. O'Malley, M. Kubeil, B. Graham, H. Stephan and L. Spiccia, *Adv. Mater.*, 2011, **23**, H18–H40.
- 9 L. M. De Leon-Rodriguez, A. J. M. Lubag, C. R. Malloy, G. V. Martinez, R. J. Gillies and A. D. Sherry, *Acc. Chem. Res.*, 2009, **42**, 948–957.
- 10 E. Terreno, D. D. Castelli, A. Viale and S. Aime, *Chem. Rev.*, 2010, **110**, 3019–3042.
- 11 C. Li, *Nat. Mater.*, 2014, **13**, 110–115.
- 12 K. M. Ward, A. H. Aletras and R. S. Balaban, *J. Magn. Reson.*, 2000, **143**, 79–87.
- 13 E. Terreno, C. Boffa, V. Menchise, F. Fedeli, C. Carrera, D. D. Castelli, G. Digilio and S. Aime, *Chem. Commun.*, 2011, **47**, 4667–4669.
- 14 Q. Wang, S. Chen, Q. Luo, M. Liu and X. Zhou, *RSC Adv.*, 2015, **5**, 1808–1811.
- 15 A. X. Li, F. Wojciechowski, M. Suchy, C. K. Jones, R. H. E. Hudson, R. S. Menon and R. Bartha, *Magn. Reson. Med.*, 2008, **59**, 374–381.
- 16 L. A. Ekanger, M. M. Ali and M. J. Allen, *Chem. Commun.*, 2014, **50**, 14835–14838.
- 17 H. Grull, S. Langereis, L. Messenger, D. D. Castelli, A. Sanino, E. Torres, E. Terreno and S. Aime, *Soft Matter*, 2010, **6**, 4847–4850.
- 18 O. M. Evbuomwan, G. Kiefer and A. D. Sherry, *Eur. J. Inorg. Chem.*, 2012, 2126–2134.
- 19 C. Khemtong, C. W. Kessinger and J. Gao, *Chem. Commun.*, 2009, 3497–3510.
- 20 H. Wei, X. Zhang, C. Cheng, S.-X. Cheng and R.-X. Zhuo, *Biomaterials*, 2007, **28**, 99–107.
- 21 H. Wei, X.-Z. Zhang, Y. Zhou, S.-X. Cheng and R.-X. Zhuo, *Biomaterials*, 2006, **27**, 2028–2034.
- 22 K. W. Y. Chan, G. Liu, X. Song, H. Kim, T. Yu, D. R. Arifin, A. A. Gilad, J. Hanes, P. Walczak, P. C. M. van Zijl, J. W. M. Bulte and M. T. McMahon, *Nat. Mater.*, 2013, **12**, 268–275.
- 23 S. Zhang, K. Zhou, G. Huang, M. Takahashi, A. Dean Sherry and J. Gao, *Chem. Commun.*, 2013, **49**, 6418–6420.
- 24 J. Zhou and P. C. M. v. Zijl, *Prog. Nucl. Magn. Reson. Spectrosc.*, 2006, **48**, 109–136.
- 25 D. E. Woessner, S. Zhang, M. E. Merritt and A. D. Sherry, *Magn. Reson. Med.*, 2005, **53**, 790–799.